

Hilbert–Huang transform analysis of periodicities in the last two solar activity cycles

D. Y. Kolotkov,^{1★} A.-M. Broomhall^{1,2★} and V. M. Nakariakov^{1,3,4★}

¹*Centre for Fusion, Space and Astrophysics, Department of Physics, University of Warwick, Coventry CV4 7AL, UK*

²*Institute of Advanced Studies, University of Warwick, Coventry CV4 7HS, UK*

³*School of Space Research, Kyung Hee University, Yongin, Gyeonggi 446-701, Korea*

⁴*Central Astronomical Observatory at Pulkovo of the Russian Academy of Sciences, St Petersburg 196140, Russia*

Accepted 2015 June 2. Received 2015 May 12; in original form 2015 March 18

ABSTRACT

We investigated periodicities associated with the last two-and-a-half solar activity cycles with the novel Hilbert–Huang transform (HHT) method. Raw data signals of five different observational proxies: the 10.7 cm radio flux intensity, the helioseismic frequency shift, and the sunspot area signals recorded from the whole solar disc, and separately from the Northern and Southern hemispheres, were expanded into a set of intrinsic modes with the ensemble empirical mode decomposition technique. Instant and mean periods of each empirical mode were obtained with the use of the Hilbert transform applied independently to each separate mode. The periodicities were allocated to three distinct groups: short-term variations (with periods shorter than 0.5 yr), quasi-biennial oscillations (with typical periods from 0.5 yr to 3.9 yr), and longer periodicities, e.g. such as the 11 yr cycle. All periodicities detected in the examined solar cycles 22–24 are consistent with the well-known results found in the earlier solar epochs. We have demonstrated that the HHT method is a good tool for characterizing periodicities in the helioseismic data, which are necessarily relatively limited in terms of their time resolution. Periodicities obtained using the helioseismic data are, nevertheless, consistent with those found in other proxies. Since helioseismic oscillations are sensitive to the solar interior, this indicates that the behaviour of surface and atmospheric magnetic activity reflects that of the Sun’s internal magnetic field. All identified intrinsic modes are seen to have clear amplitude modulation highly correlated with the 11 yr cycle. This amplitude modulation is most pronounced in the short-period modes. The short-term periodicities were found to be multiples of the shortest period, of 25 d. This ordering of the short-term periodicities is consistent with the previous findings. Signatures of the north–south asymmetry were detected in the individual hemisphere sunspot area indices. Furthermore, evidence of the last ‘extended’ solar minimum was detected too.

Key words: Sun: activity – Sun: helioseismology.

1 INTRODUCTION

The Sun’s magnetic activity varies primarily on a time-scale of 11 yr. However, both longer and shorter term periodicities are also frequently associated with solar magnetic activity (see Usoskin 2013; Bazilevskaya et al. 2014, for recent reviews). In this paper, we determine activity-related periodicities that can be extracted from data recorded over the last two-and-a-half solar cycles (from 1985 to 2014). We therefore concentrate on periodicities less than (but including) 11 yr. Periodicities in the range of 1–4 yr are often re-

ferred to as quasi-biennial oscillations (QBO; Bazilevskaya et al. 2014), while periodicities shorter than 1 yr are often referred to as Reiger-type periodicities (e.g. Boberg et al. 2002; Krivova & Solanki 2002; Ballester, Oliver & Carbonell 2004; Chowdhury & Ray 2006). The periodicities appear to be ubiquitous, being detected in activity proxies that are sensitive to the solar interior, and extending right out to the interplanetary medium (see Bazilevskaya et al. 2014, for a recent review).

Solar activity periodicities are hard to characterize: even the 11 yr cycle is known to vary in both the amplitude and length (e.g. Hathaway 2010). Usually, for the spectral analysis of long-term solar activity, Fourier transforms and other more advanced Fourier-based techniques are used. However, all of them have disadvantages associated with the a priori prescription of the basis function, e.g.

* E-mail: d.kolotkov@warwick.ac.uk (DYK); A.-M.Broomhall@warwick.ac.uk (A.-M.B); V.Nakariakov@warwick.ac.uk (VMN)

the harmonic one. Hence, such methods are highly restricted in the sense of their application to non-stationary, rather anharmonic signals. As a possible solution to this problem a so-called Krylov–Bogolyubov ‘averaging’ method was suggested. It is based on the expansion of the original signal into a set of harmonic functions with time-dependent amplitude and frequency, and was successfully applied to analysis of weakly non-linear non-stationary Wolf number data by Nagovitsyn (1997). Another method suitable for non-linear and non-stationary data processing is the proper orthogonal decomposition (POD). This tool, combined with the wavelet analysis, was used to investigate the spatio-temporal behaviour of the large time-scale green coronal emission line at 530.3 nm (Vecchio & Carbone 2008, 2009). However, they were unable to adequately describe the solar cycle using POD modes.

In this paper, we consider five measures of solar activity that are sensitive to different regions: 10.7 cm radio flux,¹ helioseismic frequency shift, and the sunspot area² signals, recorded from the whole Sun disc, as well as from the Northern and Southern hemispheres separately. The 10.7 cm radio flux (F10.7), which is a proxy for solar activity in the upper chromosphere and lower corona, and is sensitive to both strong and weak magnetic field regions (Tapping 1987). Helioseismology uses the Sun’s natural oscillations to characterize conditions beneath the surface of the Sun. It is well known that the frequencies of the helioseismic acoustic oscillations (known as *p* modes) vary throughout the 11 yr solar cycle and, therefore, can be considered as proxies of solar activity (e.g. Woodard & Noyes 1985; Elsworth et al. 1990; Pallé, Régulo & Roca Cortés 1990). One of the most obvious manifestations of solar activity on the solar surface is sunspots. Sunspot area (Hathaway 2010) provides a measure of the photospheric magnetic flux. Sunspot area has the advantage that one can consider the total sunspot area or one can consider the Northern and Southern hemispheres independently, gaining insights into the well-known north–south (NS) asymmetry (see Norton, Charbonneau & Passos 2014, for a recent review). In other words, in contrast with the other proxies considered here, sunspot area signal contains information about the spatial structure of the Sun’s activity.

While numerous studies have looked at variations on time-scales shorter than 11 yr that are present in the 10.7 cm flux and sunspot area, characterizations of the shorter term signals in helioseismic data are less abundant. For example, Simoniello et al. (2013) used a wavelet analysis to study variations in helioseismic *p*-mode frequencies and found a broad peak in the global wavelet spectrum that extended between the periods of approximately 1 and 4 yr. This broad peak covers numerous individual periodicities identified in other activity proxies. However, such a broad spectrum could also be an indication of temporal instability in the periodicity. Howe et al. (2000) used helioseismic *p* modes to identify a 1.3 yr signal in variations in the solar rotation profile at a radius of $0.72 R_{\odot}$. However, other authors were not able to verify the results (e.g. Antia & Basu 2000) and follow-up study demonstrated that the signal appeared to disappear around 2000 (Howe et al. 2011). Inherent in the problem are necessary limitations on the temporal resolution with which changes in helioseismic parameters can be determined: it is necessary to consider time series accumulated over of the order of months to allow the frequencies of the individual modes to be determined accurately and precisely.

Characterization of the helioseismic signal could help differentiate between the different models proposed to explain the QBO-like variations. Different helioseismic *p* modes are sensitive to different but overlapping regions of the solar interior, and so determining how solar cycle variations differ from mode to mode can help characterize the magnetic field in the solar interior. Such characterization has frequently been performed for the 11 yr solar cycle. For example, the observed frequency dependence in the amplitude of the solar cycle variations implies that the dominant perturbation is confined to near-surface regions (e.g. Libbrecht & Woodard 1990). Basu et al. (2012) demonstrated that the region responsible for the 11 yr perturbation may be thinner in cycle 23 than in cycle 22. Its smaller amplitude and shorter time-scale make characterization of the QBO more difficult. In this paper, we describe novel techniques that could allow better characterization of the helioseismic signal and we demonstrate that the proposed method not only successfully reproduces known results for the 10.7 cm flux and sunspot area signals, but also reveals periodicities and characteristics in the helioseismic data that are consistent with the other activity proxies. This is important as to resolve QBO variations, helioseismic data are often determined from overlapping time series and so data points are correlated, which has consequences for the significance of any determined signals. Future studies will extend this work to consider a far broader range of helioseismic modes to allow, for example, the internal depth dependence and latitudinal dependence of the QBO signals to be determined and thereby potentially enabling discrimination between different QBO models.

In this paper, we present an analysis of periodicities observed in the last two solar activity cycles with the novel Hilbert–Huang transform (HHT) technique. The main idea of the HHT is a combination of the empirical mode decomposition (EMD) of a given signal on to a set of intrinsic mode functions (IMF), based on searching for the local time-scales appearing in a signal, and the subsequent Hilbert transformation of the identified IMFs (Huang et al. 1998). In order to escape the so-called mode-mixing problem, when a signal of a similar scale appears in different IMF components, we use the noise-assisted ensemble empirical mode decomposition (EEMD), based on the EMD expansion of a given signal with statistically added white noise (Wu & Huang 2009).

The first step of this scheme, the EMD of the original signal, has already been used in a long-term solar activity data analysis. More specifically, it was employed for studying the time evolution of the radial, meridional, and east–west components of the global solar magnetic field in Vecchio et al. (2012a) by using NSO/Kitt Peak magnetic synoptic maps covering the time interval from 1976 to 2003. Fundamental time-scales of the solar magnetic field variability, such as the 22 yr cycle and QBO, were identified. The time modulations both of the interplanetary cosmic rays and of the solar neutrino flux were analysed with EMD in Vecchio et al. (2010). Vecchio et al. considered the cosmic ray flux and intensity, measured by the Charged Particles Measurements Experiment (channel P2) and by the Rome neutron monitor, respectively. The solar neutrino flux data were constructed by the combination of the measurements from the Homestake (for records from 1974 to 1994) and Super-Kamiokande (for records from 1996 to 2001) experiments. All analysed signals span the time interval from 1974 to 2001. In Vecchio et al. (2012b), a more detailed joint EMD and wavelet transform analysis of the longer cosmic ray intensity records (from 1953 to 2004), obtained with the Climax neutron monitor, was performed. Comparison of the periodicities obtained from the above-mentioned data sets with the modes derived from the sunspot area and the coronal green line signals allowed a direct

¹ <http://www.ngdc.noaa.gov/stp/space-weather/solar-data/solar-features/solar-radio/noontime-flux/penticton/>

² <http://solarscience.msfc.nasa.gov/greenwch.shtml>

connection between solar neutrinos and cosmic rays with the solar magnetic field evolution to be established. The Gnevyshev gap phenomenon was explained as the superposition of the QBO to the 11 yr cycle as well. Intrinsic modes of the monthly averaged NS sunspot area records made by the Royal Greenwich Observatory for the time interval of 129 yr from 1874 to 2003 were identified with EMD in Zolotova & Ponyavin (2007). Application of the EMD procedure allowed the separation of the NS sunspot activity into high- and low-frequency parts. This in turn led to the establishment of the amplitude and phase synchronizations of the detected high- and low-frequency components. Additionally, the HHT method was recently successfully applied to much shorter periodicities in the solar emission, such as quasi-periodic pulsations, regularly observed in solar flares (Nakariakov et al. 2010; Kolotkov et al. 2015).

In this paper, we apply the HHT technique improved by EEMD to the solar cycle proxies measured more recently, in 1985–2014. This study can be considered as a development of the works by Zolotova & Ponyavin (2007) and Vecchio et al. (2010, 2012a,b), by applying the more statistically robust EEMD technique instead of EMD, and using additional proxies, which have been analysed neither with EEMD nor with EMD before, namely the helioseismic data. In addition, we use the Hilbert transformation to reveal time-dependent instantaneous periods, naturally appearing in the detected empirical modes. The paper is structured as follows: in Section 2 the examined proxies are described in detail, Section 3 gives results of HHT analysis of them, and discussion of results and conclusions are collected in Section 4.

2 DATA

The Birmingham Solar Oscillations Network (BiSON; Davies et al. 2014) is a ground-based network of six stations that make helioseismic Doppler velocity observations of the Sun. BiSON has now been accumulating observations for over 30 yr making it the longest running helioseismic observatory, and ideal for studies of the solar cycle. Here we consider data obtained between 1985 January 1 and 2014 April 11, covering two-and-a-half solar cycles, including the recent extended minimum. The BiSON data used here benefit from improved calibration procedures, which produce higher signal-to-noise ratios (Davies et al. 2014). BiSON makes unresolved (Sun-as-a-star) observations of the Sun, meaning that only those modes with the largest horizontal spatial scales (low-degree) have detectable amplitudes in frequency spectra. However, these are the truly global modes of the Sun and so their parameters (such as frequency), which are sensitive to the magnetic field in the solar interior, can be considered as global proxies of solar activity.

In order to determine how the mode frequencies vary with time, it is necessary to divide the long time series into shorter subsets. The time subsets are then converted to Fourier power spectra in which the oscillations appear as distinct peaks. These subsets must be short enough to resolve the time variations (such as the 11 yr solar cycle) but long enough that when converted to power spectra there is sufficient resolution to accurately and precisely determine the mode frequencies. Here, we consider subsets of length 108 d with start times that are separated by 36 d. Only modes with degrees (l) in the range $0 \leq l \leq 2$ are considered, as these modes have the highest amplitudes in Sun-as-a-star data. Furthermore, only modes in the range $2400 \leq \nu \leq 3500 \mu\text{Hz}$ are considered. Again these are the most prominent modes in the frequency power spectrum, meaning their frequencies can be obtained most accurately. At lower frequencies, not only does the amplitude of the oscillations decrease but the

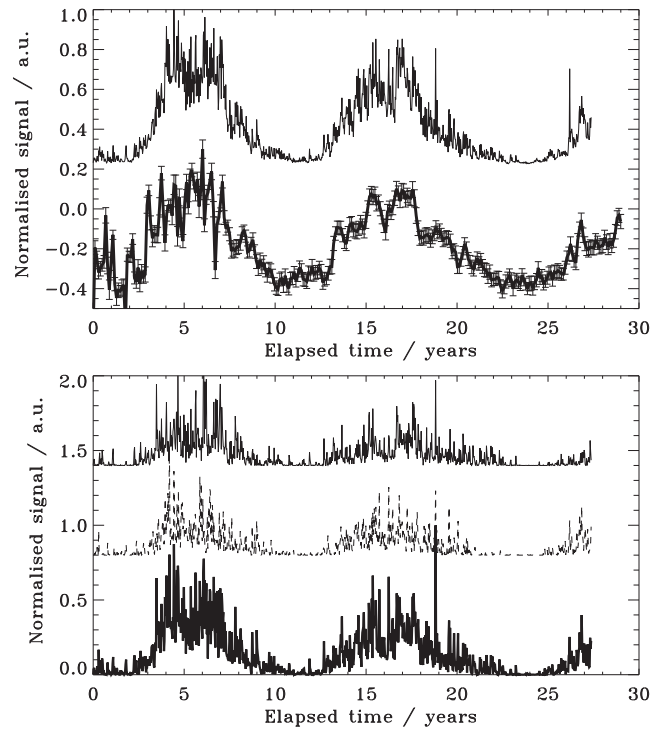


Figure 1. Upper panel: raw data signal of the 10.7 cm radio flux intensity (upper thin solid line), provided by the National Geophysical Data Center (NGDC), and the raw data of the helioseismic frequency shift with uncertainties (bottom thick solid line), detected with the BiSON. The signals are normalized to their maximum values, and the frequency shift signal is slightly shifted down for better separation. Bottom panel: sunspot area signals, recorded from the whole Sun disc (bottom thick solid line), from the Northern solar hemisphere (middle dashed line), and from the Southern hemisphere (upper thin solid line), by the Royal Observatory, Greenwich. The signals are normalized to the maximum value of the bottom signal, and signals from separate hemispheres are shifted up for better visualization. The elapsed time is measured from 1985 January 1.

change in mode frequency between solar minimum and maximum decreases significantly. At higher frequencies, the oscillations are heavily damped meaning their profile in a power spectrum is broad and therefore their frequencies cannot be obtained as precisely. The frequencies were obtained by fitting the asymmetric profile of Nigam & Kosovichev (1998) using the maximum likelihood estimation technique (Fletcher et al. 2009). The frequency shifts were then determined in the manner described in detail by Broomhall et al. (2009) and briefly outlined here. First a ‘reference’ set of frequencies was obtained by determining the average frequency of each individual mode across all subsets. For each individual subset and mode, the change in frequency compared to this reference set was determined. Finally, the average across all modes was determined for each subset. The uncertainties on the average frequencies were based on the uncertainties associated with the original fitted frequencies. The result is a time series of average frequency shift (with data points separated by 36 d) that covers approximately 29 years and is ideal for studying solar cycle-associated variations (see Fig. 1).

In addition to the helioseismic data, which can be considered as a proxy for the Sun’s magnetic field in the solar interior, we also consider the sunspot area, as observed by the Royal Greenwich Observatory (Hathaway 2010), and the Penticton 10.7 cm solar radio flux (Tapping 1987, see Fig. 1). The sunspot area is a measure of

the photospheric magnetic flux. We consider both the total sunspot area and separately the sunspot area in the Northern and Southern hemispheres. F10.7 is a proxy for the magnetic field in the upper chromosphere/lower corona and is expressed in radio flux units (RFU, $1 \text{ RFU} = 10^{-22} \text{ W m}^{-2} \text{ Hz}^{-1}$).

Although daily values of the activity proxies were initially obtained, we consider two different smoothings of the sunspot area and the 10.7 cm flux signals. The EEMD technique used in this paper becomes extremely computationally intensive if more than 1000 data points are considered. Therefore, we split the time series from 1985 January 1 to 2013 May 19 into 1000 slices of 10 d each. The 10.7 cm flux and sunspot area signals were averaged using a boxcar of width 10 d. The 10 d smoothed values were independent, i.e. each data point in the smoothed time series is separated by 10 d. However, to ensure compatibility with the helioseismic results, we also smoothed the 10.7 cm flux over the same 108 d subsets from which the helioseismic frequency shifts were obtained. This smoothing was also performed using a boxcar but this time there was some overlap: each 108 d smoothed value was separated from its predecessor by 36 d. This test, therefore, ensures compatibility with the helioseismic results in terms of the different smoothing time-scales, but also allows an assessment of the impact on the results of using overlapping, and therefore correlated data.

3 ANALYSIS

3.1 The HHT technique

The signals of the five observational proxies, shown in Fig. 1, were analysed with the HHT method, starting with the noise-assisted EEMD expansion. The value of the white noise amplitude (0.2 of standard deviation of the original signal; Wu & Huang 2009), used in the EEMD, was chosen to be comparable with the values of the helioseismic data uncertainties. We next applied the Hilbert transform separately to each of the found empirical modes to reveal the instant period time variations, designated as the Hilbert spectrum. The instantaneous period regularly varies around some average value (see Fig. 2), which is referred to as the most probable mean period of each mode.

3.2 Average periodicities

The results, obtained with the HHT analysis of the raw data signals, are summarized in Table 1. Intrinsic periodicities were found simultaneously in different proxies and were separated into three distinct groups: short-term variations (with periods shorter than 0.5 yr), QBO (with typical periods from 0.5 yr up to 3.9 yr), and longer periodicities, e.g. such as the 11 yr cycle. These mean periods were estimated from the probability histograms of the corresponding Hilbert spectra. A particular example of this technique is shown in the right-hand panel of Fig. 2. Such a histogram is calculated as the number of times each period appears in the Hilbert spectrum. For each empirical mode, this distribution has a Gaussian-like shape with a distinct peak, designated as the most probable period of the mode. The significances, σ_{peak} , of these peaks were estimated by comparing the peak height (which is unity after normalization to its maximum) with the value of the standard deviation of the whole probability histogram (see the right-hand panel of Fig. 2). All significances were found to be greater than or equal to 4.4 standard deviations. Furthermore, according to Table 1, σ_{peak} grows with increasing modal period, meaning that the Hilbert spectrum of a mode

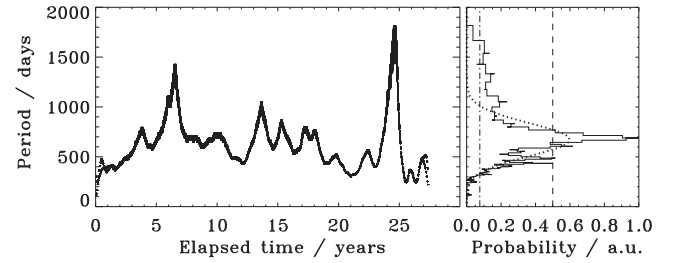


Figure 2. Left-hand panel: Hilbert spectrum, dependence of the instantaneous period upon time, of intrinsic mode 7 of the radio flux signal (see Fig. 1), shown in Fig. 3 (line (3) in the upper panel), determined with EEMD and characterized by a mean period of about 690 d (≈ 2 yr), i.e. a QBO. The elapsed time is measured from 1985 January 1. Right-hand panel: histogram (solid line), representing the most probable mean period of the Hilbert spectrum. It is calculated as the number of times each period appears in the Hilbert spectrum. The distribution has a Gaussian-like shape with the distinct peak at about 690 d (≈ 2 yr), designated as the mean most probable period of the empirical mode. The best-fitting Gaussian function of the form $y(x) = a \exp(-(x - b)^2 / 2c^2)$, where $a \approx 0.6$, $b \approx 672.8$, and $c \approx 166.3$, is shown by the dotted line; the half-level of the histogram is shown by the dashed line. The vertical dot-dashed line shows the value of standard deviation of the histogram. The probability is normalized to its maximum value.

with a longer period varies less in time, allowing the mean periodicity to be determined more accurately. The negative and positive error bars of the all obtained periods were estimated at the half-level width of the corresponding probability histogram.

3.3 Time variability of the empirical modes

Fig. 3 contains several examples of empirical intrinsic modes of the investigated raw signals, obtained with the EEMD expansion. The intrinsic modes plotted in the top panel of Fig. 3 have a mean period of 626^{+69}_{-113} d (≈ 1.7 yr) and are obtained from the sunspot area signals, recorded from the Northern solar hemisphere (line 1), and from the whole disc (line 2), and the 10.7 cm radio flux intensity, respectively. Also plotted (in the middle panel) are the modes, characterized by the average period of 903^{+133}_{-64} d (≈ 2.5 yr), obtained from the helioseismic frequency shift and the 10.7 cm radio flux intensity. Finally, in the bottom panel of Fig. 3, we show the longest 11 yr empirical modes, which were obtained using all proxies. All modes are normalized to their maximum values and are slightly shifted upwards or downwards accordingly for better visualization; hence, the information about the absolute amplitude is artificially eliminated. However, the absolute amplitudes of the 11 yr modes were found to be much greater, generally by a factor of 5, than the obtained amplitudes of shorter period modes, and this was true for all proxies examined here.

It should be noted that the QBO of the sunspot area proxies with the average period of 626 d were found only in the signals from the whole Sun disc and from the Northern hemisphere (see Table 1), and are absent in the Southern hemisphere. Accordingly one can expect that lines 1 and 2 in the upper panel of Fig. 3 demonstrate in-phase behaviour. Indeed, correlation analysis of these lines showed that the cross-correlation coefficient varies from 0.8 to 0.9 at time lags of 0.1–0.2 yr (6–12 per cent of the modal average period), except between 3 and 13 yr and between 17.1 and 18.6 yr, where the modes were artificially corrupted by the decomposition process. The time lags found are within the error bars of the estimation, generated by the EEMD. Similar in-phase behaviour was shown by the intrinsic modes of the sunspot area signals with a shorter average period

Table 1. Intrinsic periodicities of the signals of five solar cycle proxies, estimated with HHT technique. The periods are measured in days, and their significances σ_{peak} are estimated in units of the standard deviations, calculated separately for each probability histogram of each Hilbert spectrum.

10.7 cm radio flux		Frequency	Sunspot area recorded from			Average
108 d smooth Period (d)/ σ_{peak}	10 d smooth Period (d)/ σ_{peak}	shift Period (d)/ σ_{peak}	whole Sun Period (d)/ σ_{peak}	Northern hemisphere Period (d)/ σ_{peak}	Southern hemisphere Period (d)/ σ_{peak}	period Period (d)
	$22^{+21}_{-2}/5.5$		$23^{+11}_{-2}/5.9$	$25^{+15}_{-5}/4.8$	$28^{+6}_{-7}/6.6$	25^{+7}_{-2}
	$46^{+22}_{-8}/6$		$43^{+24}_{-10}/5.6$	$40^{+19}_{-7}/6.1$	$48^{+9}_{-13}/6.6$	44^{+10}_{-5}
			$80^{+52}_{-24}/6.5$	$75^{+48}_{-24}/5.1$	$71^{+45}_{-16}/5.4$	75^{+28}_{-13}
	$96^{+18}_{-29}/5.8$	$101^{+36}_{-11}/5.5$		$98^{+106}_{-28}/5.6$		98^{+38}_{-14}
			$128^{+70}_{-28}/5.2$		$125^{+32}_{-41}/5.5$	127^{+38}_{-25}
	$140^{+120}_{-40}/5.6$				$160^{+30}_{-25}/6.9$	150^{+62}_{-24}
		$216^{+162}_{-50}/4.4$	$198^{+105}_{-31}/6.4$	$214^{+39}_{-70}/7$	$222^{+72}_{-24}/8.3$	213^{+52}_{-24}
$256^{+6}_{-37}/6.4$	$290^{+81}_{-95}/7.4$			$294^{+141}_{-47}/8.7$		292^{+81}_{-53}
$360^{+122}_{-77}/5.4$	$328^{+149}_{-15}/10$	$378^{+74}_{-35}/6$	$408^{+47}_{-148}/8.3$	$435^{+154}_{-145}/8.8$	$426^{+9}_{-98}/10.5$	395^{+46}_{-46}
$708^{+215}_{-163}/4.4$	$690^{+80}_{-200}/13$		$625^{+65}_{-240}/9.5$	$563^{+178}_{-128}/10.6$		626^{+69}_{-113}
$885^{+177}_{-200}/7.6$	$833^{+417}_{-63}/14$	$965^{+46}_{-233}/7.4$	$930^{+180}_{-190}/11.1$	$952^{+477}_{-82}/14.5$	$833^{+76}_{-33}/17.7$	903^{+133}_{-64}
$1180^{+337}_{-214}/7.1$	$1110^{+710}_{-340}/11.3$	$1250^{+520}_{-239}/6.8$	$1538^{+280}_{-538}/12.9$	$1818^{+182}_{-151}/18.4$	$1400^{+268}_{-223}/15.8$	1423^{+196}_{-146}
$4248^{+2832}_{-1213}/7$	$4000^{+2670}_{-665}/23.2$	$4250^{+2830}_{-710}/12.2$	$4500^{+2170}_{-1160}/17.3$	$4000^{+1000}_{-667}/23.9$	$4000^{+2667}_{-667}/19.1$	4150^{+1058}_{-357}

of 127 d (see Fig. 4). In this case, the obtained periodicities were found to appear simultaneously in the whole Sun signal and in the Southern hemisphere only, and are absent in the signal from the Northern hemisphere.

The modes with a mean period of 903 d, obtained from the helioseismic frequency shifts and the 10.7 cm flux and presented in the middle panel of Fig. 3, show rather out-of-phase behaviour during the maximum of cycle 22, but are in phase during the maximum of cycle 23. Moreover, in-phase behaviour of those modes is also seen at the very beginning of the current 24th solar cycle. The quasi-biennial and longer periodicities obtained with the 108 d, overlapping smoothed 10.7 cm flux data were found to be consistent with those obtained for the 10 d smoothed data. As one might expect, short-term periodicities were not detected in the 108 d smoothed data because the time resolution is not fine enough (see Table 1). The middle panel of Fig. 3 allows comparison of one of the intrinsic modes found in both the 10 and 108 d smoothed 10.7 cm flux data. It is clear that the agreement is predominantly very good. Table 1 allows comparison of the mean periods of the determined intrinsic modes. The obtained mean periods are also in good agreement (all within 1σ), and, although the modes are less significant in the 108 d smoothed data, they are all still significant. This indicates that the EEMD technique is not adversely affected by the fact that correlated data were used and, therefore, the intrinsic modes obtained from the helioseismic data can be trusted.

The 11 yr cycle is clearly detected in the all proxies and is shown in the bottom panel of Fig. 3. The signatures of the so-called extended last minimum are well pronounced in these curves too. It is also clearly seen that 11 yr maxima of the sunspot area signals recorded separately from the Northern and Southern hemispheres are slightly shifted with respect to each other.

Fig. 4 contains the most representative examples of the identified short-term empirical modes, with mean periods of 25 and 127 d. These modes are seen to have a clear amplitude modulation that is highly correlated with the corresponding 11 yr cycle, appearing as a sudden increase of the modal amplitude during the 11 yr cycle maximum. Moreover, the modal patterns observed around solar maxima exhibit additional amplitude modulations, with periodicities much

shorter than 11 yr, and demonstrate a wave train behaviour. Rapid intensive fluctuations (also called ‘surges’) were also found to occur during the solar maxima and are particularly pronounced in the 25 d period modes. One such surge, appearing at the vicinity of 19 yr of the elapsed time (the end of the 23rd solar cycle, see Fig. 4), was detected in all short-term modes and corresponds to the beginning of the extended minimum between cycles 23 and 24. All of the fine properties described above are common to all short-term variations, as well as partly appearing in several of the shortest QBO modes, and require further, more detailed investigations.

4 DISCUSSION AND CONCLUSIONS

We have presented the spectral analysis of periodicities in the last two-and-a-half solar activity cycles performed by the HHT method, considering the following solar observational proxies: helioseismic frequency shift, 10.7 cm radio flux, and sunspot area signals from the whole Sun disc, as well as from the Northern and Southern hemispheres separately. Similar periodicities were determined in the different proxies independently and simultaneously, and were distinguished into three groups: short-term variations (with periods shorter than 0.5 yr), likely related to the so-called Reiger-type periodicities (Rieger et al. 1984); QBO (Bazilevskaya et al. 2014), having periods in the range of 0.5–3.9 yr; and longer periodicities, such as the 11 yr cycle. Hence, all detected periodicities are consistent with previous, well-known results. In particular, using the above listed proxies, which are different from the ones analysed with EMD in Vecchio et al. (2010, 2012a,b), we extracted the same types of periodicities, such as the QBO and 11 yr modes. Furthermore, our results were obtained with the noise-assisted EEMD, which provides more statistically robust results. The fact that similar periodicities are independently detected in different observational proxies confirms their physical nature. In addition, similar periodicities of about 27 d, 79 d, 1.3 yr, and 1.7 yr, as well as the 11 yr cycle, were very recently detected with EMD in the records of the daily coronal index of Fe XIV emission from 1939 to 2008 (Deng et al. 2015).

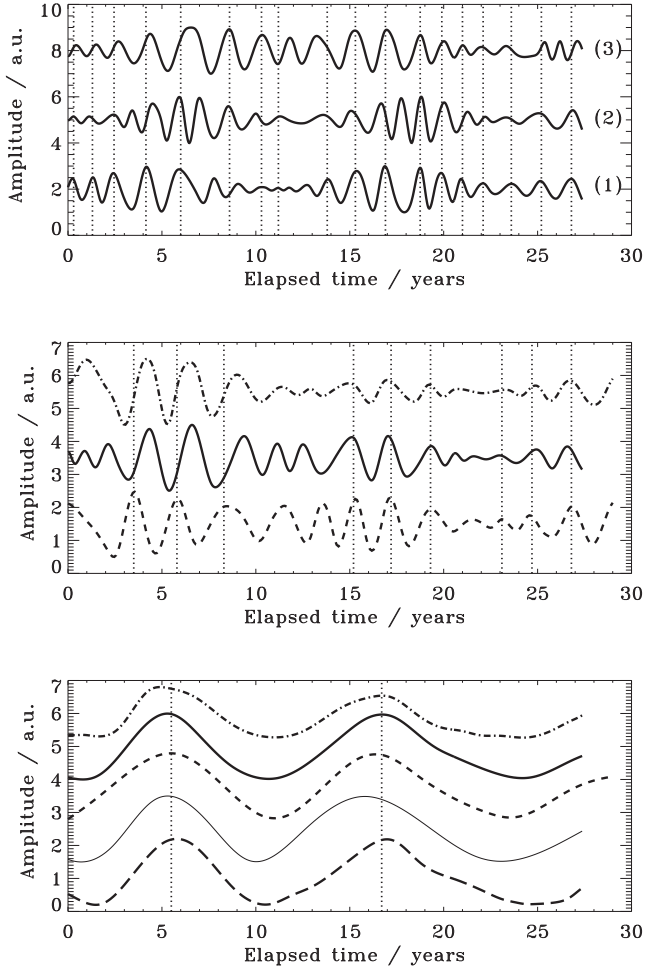


Figure 3. Upper panel: intrinsic empirical modes, characterized by the average period of 626^{+69}_{-113} d (≈ 1.7 yr), of the sunspot area signal, recorded from the Northern hemisphere (line 1), the sunspot area signal, recorded from the whole Sun disc (line 2), and the 10.7 cm radio flux intensity (line 3). Middle panel: intrinsic empirical modes, characterized by the average period of 903^{+133}_{-64} d (≈ 2.5 yr), of the helioseismic frequency shift (bottom dashed line), and of the 10.7 cm radio flux intensity obtained from the signals smoothed over 10 d (middle solid line), and over 108 d (upper dot-dashed line). Bottom panel: the longest 11 yr empirical modes of the sunspot area signal recorded from the Southern solar hemisphere (bottom long-dashed line), the sunspot area signal, recorded from the Northern hemisphere (thin solid line), the sunspot area signal, recorded from the whole Sun disc (thick solid line), and the 10.7 cm radio flux intensity (upper dot-dashed line). Dotted vertical lines in all the panels show *in-phase/out-of-phase* behaviour of the modes. All signals are normalized to their maximum values and shifted accordingly to provide better visualization. The elapsed time is measured from 1985 January 1.

The shortest detected period of 25^{+7}_{-2} d is clearly associated with the monthly solar rotation. It was detected in all observational proxies, except the helioseismic frequency shift (see Table 1), because the helioseismic frequency shifts are determined from time series of 108 d in length meaning it is not possible to resolve such short periodicities. Furthermore, the next identified Reiger-type periods, such as 44^{+10}_{-5} , 75^{+28}_{-13} , 98^{+38}_{-14} , 127^{+38}_{-25} , and 150^{+62}_{-24} d, are seen to be the approximate multiples of 25 d. This ordering was previously detected in Bai (2003), where periodicities of the solar-flare occurrence rate during of cycles 19–23 were analysed. This finding

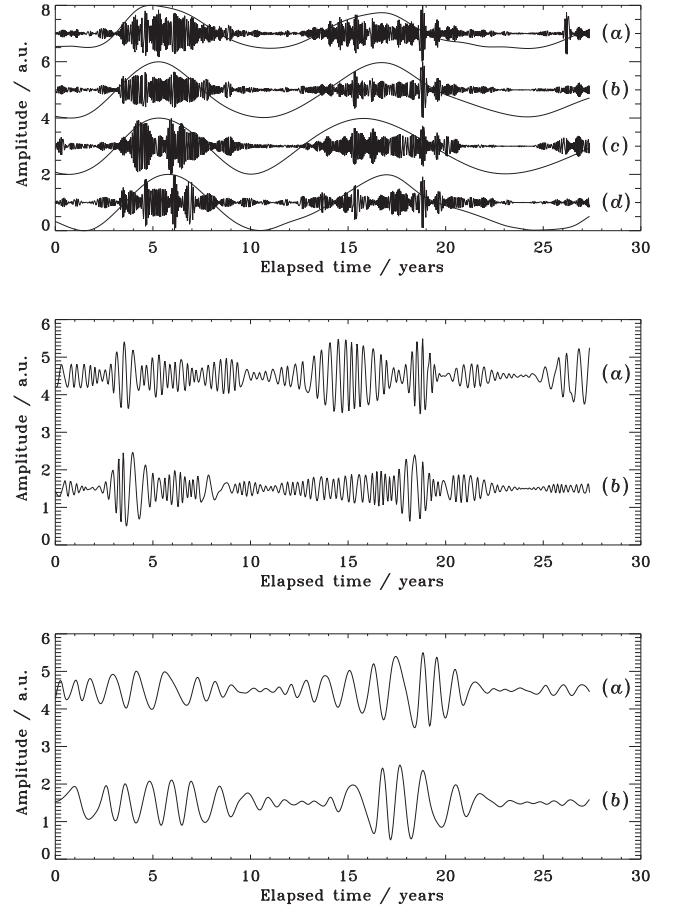


Figure 4. Upper panel: intrinsic empirical modes, characterized by the average period of 25^{+7}_{-2} d, of the 10.7 cm radio flux intensity (a); of the total sunspot area (b), and from the Northern hemisphere (c), and from the Southern hemisphere (d). The overplotted thin solid lines show corresponding 11 yr intrinsic modes. Middle panel: intrinsic empirical modes, characterized by the average period of 127^{+38}_{-25} d, of the sunspot area signal, recorded from the whole Sun disc (a), and from the Southern hemisphere (b). All signals are normalized to their maximum values and shifted accordingly to provide better visualization. The elapsed time is measured from 1985 January 1. Bottom panel: empirical modes of the Northern (a) and Southern (b) sunspot area signals, having mean periods of 435 and 426 d, respectively.

was claimed to support the idea that the 25 d period is one of the fundamental periods of the Sun, and various observational proxies (e.g. the sunspot area and the 10.7 cm radio flux) of the solar magnetic activity often exhibit periodicities at its multiples (Bai & Sturrock 1991). The mechanisms possibly responsible for such an ordering remain uncertain. The 25 d periodicity is likely to be related to the solar rotation rate and the associated evolution of the solar photospheric magnetic field. In particular in Knaack, Stenflo & Berdyugina (2005) a similar ordering of the Reiger-type periodicities was found in the analysis of the monthly variations of the photospheric magnetic field.

Some of the identified modes are seen to have the 11 yr modulation of their amplitudes, appearing as a rapid increase in the modal amplitude in phase with the 11 yr solar cycle maxima and subsequent decrease during solar minima. This modulation is indeed highly correlated with the extracted 11 yr modes, and is mainly pronounced in the shorter period modes (all Reiger-type periodicities and several short-period QBO modes), while the longer period modes were found to have rather stable amplitudes. Similar 11 yr

amplitude modulation of the short-period modes has been found in earlier solar epochs: Zolotova & Ponyavin (2007) analysed sunspot area signals from the Northern and Southern hemispheres for the time interval of 129 yr from 1874 to 2003 with EMD. The authors separated their obtained results into the high- and low-frequency parts. The common signal, constructed as the sum of the high-frequency components, having periods up to 3 yr, showed evident 11 yr amplitude synchronization as a result of 11 yr cycle modulation for both hemispheres. Usage of the EEMD expansion in our work, which prevents the mode leakage artefact, allowed us to determine such 11 yr amplitude modulation in each individual high-frequency mode. This in turn led to the revealing of fine structures, such as the rapid intensive surges and additional amplitude modulation of the modes in the form of oscillating trains. These findings support the fact that the large-scale magnetic field related to the 11 yr solar cycle consists of small-scale magnetic elements, which was observed e.g. in Benevolenskaya (2010) with the Solar & Heliospheric Observatory (SOHO)/Michelson Doppler Imager (MDI) synoptic maps for cycle 23. Such small-scale magnetic elements were found to demonstrate quasi-periodic behaviour of their magnetic flux with extremely short periods ranging from a few hours to a few days. The strong coupling of the fine structures in Fig. 4 with 11 yr cycle also indicates their production rather by the global dynamo, e.g. via the turbulent cascade, rather than by the local dynamo. Such a discrimination between the dynamo models is allowed to be established because of the fact that the local dynamo is essentially decoupled from the solar activity and contributes to a background quiet-Sun magnetic field only (Stenflo 2013).

The use of the sunspot area signals simultaneously from the whole visible disc, as well as from the Northern and Southern hemispheres separately, allowed one to analyse the spatial structure of the Sun's activity. The empirical mode with an average period of 626 d, which is detected in the total-Sun sunspot area can be associated with a signal that is presented in only the Northern hemisphere. Similarly, the empirical mode with an average period of 127 d which is also found in the total-Sun sunspot area can be associated with a signal from only the Southern hemisphere (see Table 1). These findings can be considered as additional signatures of the NS asymmetry in the solar hemisphere evolution (e.g. Badalyan & Obridko 2011). Similarly, in Zolotova & Ponyavin (2007) the above-described high-frequency components of the sunspot area signals decomposed via EMD were found to demonstrate randomly mixed phase behaviour, supporting the general idea that the Northern and Southern solar hemispheres evolve rather differently. In our paper, the application of the EEMD method allowed us to specify the two particular modes (with average periods of 626 and 127 d) from the above-mentioned high-frequency range, demonstrating clear indications of the NS asymmetry. In contrast, all identified empirical modes from the low-frequency part in Zolotova & Ponyavin (2007) (with periods greater than 3 yr) were found to be well synchronized in phase, i.e. signatures of NS asymmetry were absent. The latter is generally in good agreement with our findings. Further evidence of the NS asymmetry obtained in our work is that the maxima of the detected 11 yr modes, corresponding to the phases of solar activity maxima, in sunspot area signals from the Northern and Southern hemispheres are shifted in time with respect to each other. This means slightly different periods of time when hemispheres exhibit maximum magnetic activity. This effect is extremely well known and observed (see Norton et al. 2014, for a recent review).

The mean periodicities reported in Section 3.2 were estimated as the most probable periods of the empirical modes with usage of the averaging histogram technique described above. However,

application of the HHT method allows one to determine actual time variability of each modal period too. All modes were found to have rather unstable instantaneous periods, differently varying around a mean value from one cycle of oscillation to another (see examples of modes in Figs 3 and 4). More specifically, e.g., the empirical mode with the mean period of 426 d of the Southern sunspot area signal (Fig. 4) exhibits quite stable period behaviour throughout nearly the entirety of cycle 22, while the modal periodicity changes dramatically (up to values of about 600 d for at least three periods of oscillation) during cycle 23. Such strong deviations of the instant period from the mean value are occasionally observed. In this instance, that is why the separate mode with the mean period of about 600 d in the sunspot area signal from the Southern hemisphere was not detected in the work. It is also possible that the number of modes identified in this work was being limited by the threshold that controls when the 'sifting' process is terminated in each EMD trial, which is determined by the level of the standard deviation from the previous iteration. We recall that the EEMD methodology applied was identical for all observational proxies, including the value of the deviation threshold of 0.3. Hence, the fact that the number of modes found for the Northern hemisphere differs from the number found for the Southern hemisphere reflects natural intrinsic features of the original data sets. This value was taken from the interval 0.1–0.4 originally recommended by Huang et al. (1998). Therefore, as an additional check the whole procedure was repeated for the Southern sunspot area signal with a threshold value of 0.1, three times less than the original value. This gave the same set of modes, with absolutely identical periods to the previous results, i.e. convergence of the method is evidently reached for both threshold levels.

We have demonstrated that the EEMD technique is an effective tool for characterizing variations in the properties of helioseismic parameters on time-scales shorter than 11 yr, and, therefore, for characterizing the variations in the Sun's internal magnetic field. Good agreement is found with the other activity proxies, and this is true for both those smoothed over independent 10 d boxcars and those smoothed over overlapping 108 d boxcars. This is important since helioseismic investigations of the Sun's activity cycles frequently consider overlapping, and therefore, correlated data, which can affect the significance of any determined signals. We have demonstrated that the quasi-biennial signal in the helioseismic data can be split into two main modes, with periods of 965^{+46}_{-233} and 1250^{+520}_{-239} d. Both lie within the broad peak found using wavelet techniques by Simoniello et al. (2013), and the large uncertainties indicate some instability in the periodicities. However, the Hilbert spectrum indicates that these instabilities primarily arise from epochs around solar minimum, when the amplitudes of the signals are relatively low. An extension to this work will be to consider a broader range of helioseismic modes, in order to characterize the depth and latitudinal dependence of these signals.

Finally, thanks to the fact that the EMD technique is originally based on the searching for the local time-scales appearing in the signal, and, hence, is suitable for analysing essentially anharmonic signals, signatures of the so-called extended last solar minimum were successfully established in the work. They are clearly pronounced in all extracted 11 yr modes as the sudden changes in the slopes of the 11 yr modes during the decaying phase of the last solar maximum.

ACKNOWLEDGEMENTS

We thank the Birmingham Solar Oscillations Network, NOAA NGDC, and the Royal Observatory (Greenwich) for making their

data freely available. This work is supported by the European Research Council research project 321141 *SeismoSun* (VMN), the BK21 plus programme through the National Research Foundation funded by the Ministry of Education of Korea (VMN), and the Russian Foundation for Basic Research project 13-02-00044 (VMN). A-MB thanks the Institute of Advanced Study, University of Warwick for their financial support.

REFERENCES

- Antia H. M., Basu S., 2000, *ApJ*, 541, 442
- Badalyan O. G., Obridko V. N., 2011, *New Astron.*, 16, 357
- Bai T., 2003, *ApJ*, 591, 406
- Bai T., Sturrock P. A., 1991, *Nature*, 350, 141
- Ballester J. L., Oliver R., Carbonell M., 2004, *ApJ*, 615, L173
- Basu S., Broomhall A.-M., Chaplin W. J., Elsworth Y., 2012, *ApJ*, 758, 43
- Bazilevskaya G., Broomhall A.-M., Elsworth Y., Nakariakov V. M., 2014, *Space Sci. Rev.*, 186, 359
- Benevolenskaya E. E., 2010, *Astron. Nachr.*, 331, 63
- Boberg F., Lundstedt H., Hoeksema J. T., Scherrer P. H., Liu W., 2002, *J. Geophys. Res.*, 107, 1318
- Broomhall A.-M., Chaplin W. J., Elsworth Y., Fletcher S. T., New R., 2009, *ApJ*, 700, L162
- Chowdhury P., Ray P. C., 2006, *MNRAS*, 373, 1577
- Davies G. R., Chaplin W. J., Elsworth Y., Hale S. J., 2014, *MNRAS*, 441, 3009
- Deng L. H., Li B., Xiang Y. Y., Dun G. T., 2015, *J. Atmos. Sol.-Terr. Phys.*, 122, 18
- Elsworth Y., Howe R., Isaak G. R., McLeod C. P., New R., 1990, *Nature*, 345, 322
- Fletcher S. T., Chaplin W. J., Elsworth Y., New R., 2009, *ApJ*, 694, 144
- Hathaway D. H., 2010, *Living Rev. Sol. Phys.*, 7, 1
- Howe R., Christensen-Dalsgaard J., Hill F., Komm R. W., Larsen R. M., Schou J., Thompson M. J., Toomre J., 2000, *Science*, 287, 2456
- Howe R., Komm R., Hill F., Christensen-Dalsgaard J., Larson T. P., Schou J., Thompson M. J., Toomre J., 2011, *J. Phys.: Conf. Ser.*, 271, 012075
- Huang N. E. et al., 1998, *R. Soc. Lond. Proc. Ser. A*, 454, 903
- Knaack R., Stenflo J. O., Berdyugina S. V., 2005, *A&A*, 438, 1067
- Kolotkov D. Y., Nakariakov V. M., Kupriyanova E. G., Ratcliffe H., Shibasaki K., 2015, *A&A*, 574, A53
- Krivova N. A., Solanki S. K., 2002, *A&A*, 394, 701
- Libbrecht K. G., Woodard M. F., 1990, *Nature*, 345, 779
- Nagovitsyn Y. A., 1997, *Astron. Lett.*, 23, 742
- Nakariakov V. M., Inglis A. R., Zimovets I. V., Foullon C., Verwichte E., Sych R., Myagkova I. N., 2010, *Plasma Phys. Control. Fusion*, 52, 124009
- Nigam R., Kosovichev A. G., 1998, *ApJ*, 505, L51
- Norton A. A., Charbonneau P., Passos D., 2014, *Space Sci. Rev.*, 186, 251
- Pallé P. L., Régulo C., Roca Cortés T., 1990, in Osaki Y., Shibahashi H., eds, *Lecture Notes in Physics*, Vol. 367, Progress of Seismology of the Sun and Stars. Springer-Verlag, Berlin, p. 129
- Rieger E., Kanbach G., Reppin C., Share G. H., Forrest D. J., Chupp E. L., 1984, *Nature*, 312, 623
- Simoniello R., Jain K., Tripathy S. C., Turck-Chièze S., Baldner C., Finsterle W., Hill F., Roth M., 2013, *ApJ*, 765, 100
- Stenflo J. O., 2013, *A&AR*, 21, 66
- Tapping K. F., 1987, *J. Geophys. Res.*, 92, 829
- Usoskin I. G., 2013, *Living Rev. Sol. Phys.*, 10, 1
- Vecchio A., Carbone V., 2008, *ApJ*, 683, 536
- Vecchio A., Carbone V., 2009, *A&A*, 502, 981
- Vecchio A., Laurenza M., Carbone V., Storini M., 2010, *ApJ*, 709, L1
- Vecchio A., Laurenza M., Meduri D., Carbone V., Storini M., 2012a, *ApJ*, 749, 27
- Vecchio A., Laurenza M., Storini M., Carbone V., 2012b, *Adv. Astron.*, 2012, 834247
- Woodard M. F., Noyes R. W., 1985, *Nature*, 318, 449
- Wu Z., Huang N. E., 2009, *Adv. Adapt. Data Anal.*, 1, 1
- Zolotova N. V., Ponyavin D. I., 2007, *Sol. Phys.*, 243, 193

This paper has been typeset from a \LaTeX file prepared by the author.